AGU PUBLICATIONS

Global Biogeochemical Cycles

RESEARCH ARTICLE
10.1002/2016GB005617

Key Points:
- We examined the simulated dissolved O_2 in the North Atlantic Ocean and its centennial trends in a subset of CMIP5 ESMs
- While dissolved O_2 broadly decreases in the North Atlantic under a warming climate, simulated O_2 trends are highly variable
- The patchiness of the O_2 trend reflects changes in solubility and AOU associated with the changes in ocean convection and the shifts in circulation pathways

Correspondence to:
F. Tagklis,
ftagklis3@gatech.edu

Citation:
Tagklis, F., A. Bracco, and T. Ito (2017), Physically driven patchy O_2 changes in the North Atlantic Ocean simulated by the CMIP5 Earth system models, *Global Biogeochem. Cycles*, *31*, 1218–1235, doi:10.1002/2016GB005617.

Received 28 DEC 2016
Accepted 18 JUL 2017
Accepted article online 22 JUL 2017
Published online 10 AUG 2017

Physically driven patchy O_2 changes in the North Atlantic Ocean simulated by the CMIP5 Earth system models

F. Tagklis[1], A. Bracco[1], and T. Ito[1]

[1]Earth and Atmospheric Sciences, Georgia Institute of Technology, Atlanta, Georgia, USA

Abstract The subpolar North Atlantic is a key region for the oceanic uptake of heat, oxygen, and carbon dioxide. Centennial oxygen (O_2) changes are investigated in the upper 700 m of the North Atlantic Ocean using a subset of Earth system models (ESMs) included in the Coupled Model Intercomparison Project phase 5. The climatological distributions of dissolved O_2 averaged for the recent past period (1975–2005) are generally well captured, although the convective activity differs among the models in space and strength, and most models show a cold bias south of Greenland. By the end of the twenty-first century, all models predict an increase in depth-integrated temperature of 2–3°C, resultant solubility decrease, weakened vertical mass transport, decreased nutrient supply into the euphotic layer, and weakened export production. Despite an overall tendency of the North Atlantic to lose oxygen, patchy regions of O_2 increase are observed due to the weakening of the North Atlantic Current (NAC) causing a regional solubility increase (the warming hole effect) and a decrease in the advection of subtropical, low-O_2 waters into the subpolar regions (the nutrient stream effect). Additionally, a shift in the NAC position contributes to localized O_2 changes near the boundaries of water masses. The net O_2 change reflects the combination of multiple factors leading to highly heterogeneous and model-dependent patterns. Our results imply that changes in the strength and position of the NAC will likely play crucial roles in setting the pattern of O_2 changes in future projections.

1. Introduction

Marine ecosystems will likely face multiple stressors as a consequence of the increasing anthropogenic emissions of CO_2 and of the induced climate warming in this and coming centuries. The oceans are "warming up, turning sour, and losing breath" as summarized by *Gruber* [2011]. Temperature increase, ocean acidification, and ocean deoxygenation are global-scale phenomena with far-reaching influences on the ecosystem and biogeochemical cycling. Ocean deoxygenation, i.e., the decline of dissolved oxygen (O_2) from the water column, is the least understood problem among the three, despite its profound influence on marine habitat and redox-sensitive biogeochemical tracers [*Doney et al*., 2012; *Feely et al*., 2004; *Grantham et al*., 2004; *Gray et al*., 2002; *Kleypas et al*., 2006, 1999; *Orr et al*., 2005; *Poertner and Knust*, 2007].

In a warming climate, the higher temperature of seawater decreases the solubility of oxygen. Additionally, upper ocean stratification may increase due to the surface warming, melting of polar ice cap at high latitudes, and an increase in precipitation, weakening the ventilation of well-oxygenated surface waters into the ocean interior [*Bopp et al*., 2002; *Froelicher et al*., 2009; *Matear et al*., 2000; *Plattner et al*., 2002; *Sarmiento et al*., 1998]. Earth system model (ESM) simulations indeed predict a strong sensitivity of ocean's O_2 content to climate warming, suggesting a significant decline in global O_2 inventory by the year 2100 especially in the extratropical thermocline [*Keeling et al*., 2010]. Regional differences, however, remain significant among models [*Bopp et al*., 2013; *Cocco et al*., 2013].

The reinforcing mechanisms above, thermally driven decrease of solubility and stratification-driven decrease of ocean ventilation, can be particularly important in regions of deepwater formation such as the subpolar North Atlantic. Convective mixing is the most important mechanism by which the water column is ventilated and oxygenated [*Kortzinger et al*., 2004]. For example, in the Labrador Sea (LS), deep convection mixes the surface waters to depths exceeding, at times, 2000 m [*Clarke and Gascard*, 1983; *Lazier et al*., 2002; *Lazier*, 1980; *Yashayaev*, 2007a, 2007b; *Yashayaev et al*., 2007] and forms the fresh and cold, highly oxygenated dense water mass, the Labrador Sea Water (LSW). The LS is a highly dynamic region for the biogeochemical tracers. The historic O_2 observations for the last 60 years do not yet exhibit a statistically significant trend but are dominated by interannual and decadal variability, indicating direct linkages between the strength of convective mixing, ventilation, and oxygen concentrations [*van Aken et al*., 2011]. For the entire North Atlantic,

Table 1. CMIP5 Modeling Groups and Model Names

Modeling Group/Center	Model Name	Reference
NOAA Geophysical Fluid Dynamics Laboratory (NOAA GFDL)	GFDL-ESM2M GFDL-ESM2G	*Dunne et al.* [2013]
Institute Pierre-Simon Laplace (IPSL)	IPSL-CM5A-LR IPSL-CMA-MR	*Dufresne et al.* [2013]
Met Office Fluid Hadley Center (MOHC)	HadGEM2-ES HadGEM2-CC	*Collins et al.* [2011] *Jones et al.* [2011]
Max Plank Institute for Meteorology (MPI)	MPI-ESM-LR MPI-ESM-MR	*Giorgetta et al.* [2013]
Community Earth System Model Contributors (CESM1)	CESM1-BGC	*Long et al.* [2013] *Moore et al.* [2013]
Norwegian Climate Centre (NCC)	NorESM1-ME	*Bentsen et al.* [2013]

the basin-scale O_2 inventory is also relatively constant but consists of compensating changes within the basin likely due to the circulation variability [*Stendardo and Gruber*, 2012]. However, unabated warming of the Arctic will continue melting of both Arctic sea ice [*Gillett et al.*, 2008] and terrestrial glaciers over Greenland [*Mernild and Liston*, 2012; *Rignot et al.*, 2008], with the end result that more freshwater can converge into the Labrador Sea [*Dickson et al.*, 2007] and possibly influence convective rates in the future [*Boning et al.*, 2016; *Luo et al.*, 2016; *Stouffer et al.*, 2006]. The LSW spreads across the northwest Atlantic at mid-depths [*Bower et al.*, 2009; *Curry et al.*, 1988; *Talley and McCartney*, 1982], flowing southward as a component of the North Atlantic Deep Water. Thus, the oxygen trends and variability in the LS can impact throughout the subpolar North Atlantic the global deep oceans. A present concern is if, when, and how a slowdown in deepwater formation in the North Atlantic will reduce the oxygen input to the deep ocean.

The primary objective of this study is to investigate the mechanisms driving the regional trends of dissolved oxygen in the subtropical and subpolar North Atlantic in the context of the state-of-the-art ESMs from the Coupled Model Intercomparison Project phase 5 (CMIP5). Both ocean-only and coupled climate models display large biases and divergent behavior in simulating the formation of deepwater masses and their variability [*Canuto et al.*, 2004; *Danabasoglu et al.*, 2014, 2016; *MacMartin et al.*, 2013]. We will, therefore, begin our investigation by testing the ability of the ESMs to reproduce the present mean state of relevant physical and biogeochemical variables. Particular attention will be paid to the representation of the convection and hydrographic structure in the North Atlantic. We do not expect the CMIP5 models to reproduce the trajectories of the climate and biogeochemical variability perfectly, but we aim at evaluating the linkages between physical climate and biogeochemical variables and how similar or different they are across the models. We will then move on to analyze the model projections to the end of the twenty-first century focusing on commonalities about models and causes for divergence.

2. Data and Methods

We analyze a subset of CMIP5 ESMs used for the Intergovernmental Panel on Climate Change Fifth Assessment Report for which all the variables of interest are available. We examine the transient simulations from 1850 to 2100 by combining the historical integrations and future projections based on the Representative Concentration Pathway 8.5 scenario [*Riahi et al.*, 2011; *Taylor et al.*, 2012]. The CMIP5 ESMs used in this study are summarized in Table 1. The list includes the Community Earth System Model, CESM1-BGC [*Long et al.*, 2013; *Moore et al.*, 2013]; two versions of the Geophysical Fluid Dynamics Laboratory (GFDL) Earth system model, GFDL-ESM2G and GFDL-ESM2M [*Dunne et al.*, 2013]; two versions of the Hadley Center Global Environment Model version 2, HadGEM2-ES and HadGEM2-CC [*Collins et al.*, 2011]; two versions of the Institute Pierre Simon Laplace model, IPSL-CM5A-LR and IPSL-CM5A-MR [*Dufresne et al.*, 2013]; two versions of the Max Plank Institute model, MPI-ESM-LR and MPI-ESM-MR [*Giorgetta et al.*, 2013]; and NorESM1-ME [*Bentsen et al.*, 2013]. GFDL-ESM2G and GFDL-ESM2M differ in their ocean module and vertical coordinate system with ESM2M using depth-based coordinates and the Modular Ocean Model and ESM2G using isopycnal coordinates and the Generalized Ocean Layered Model [*Adcroft and Hallberg*, 2006]. The same atmospheric component is used for both versions. HadGEM2-CC increases

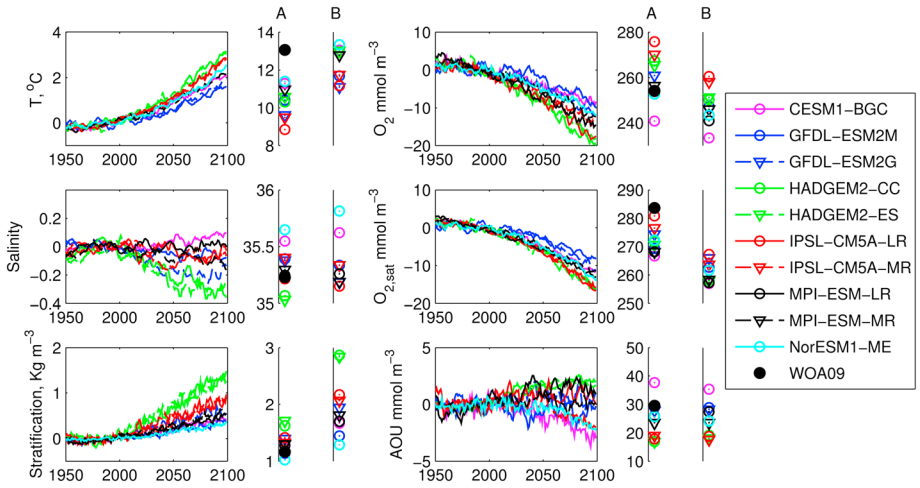

Figure 1. Volume-weighted mean time series anomalies (0–700 m) over the North Atlantic (22°N–73°N) of temperature (*T*), salinity (*S*), stratification, dissolved oxygen, oxygen saturation (O_{2sat}), and apparent oxygen utilization (AOU) over the period 1950–2100. The stratification index is defined as the density difference between 700 m and surface. Mean values are also shown in the past and projected intervals 1975–2005 (period A) and 2070–2100 (period B).

the vertical discretization of the atmospheric module from the 38 layers in HadGEM2-ES to 60 but does not include the atmospheric chemistry scheme used in the –ES version. IPSL-A-LR and IPSL-A–MR use different resolution in the atmospheric module (1.875° × 3.75° in the LR for low resolution and 1.25° × 2.5° in the MR for medium resolution). Finally, the MPI-ESM-MR configuration doubles the number of levels in the atmosphere and decreases the horizontal grid spacing of the ocean, compared to the LR setup.

The three-dimensional and annually averaged fields analyzed in this study are first interpolated horizontally onto a common domain of 1° × 1° longitude-latitude grid and vertically onto 33 depth levels. The variables we focus on are dissolved oxygen (O_2), temperature *T*, salinity *S*, particulate organic carbon export (EP), and the horizontal velocities (*u*, *v*). Further, potential density, stratification, and oxygen saturation O_{2sat} are calculated from *T* and *S*.

Regarding oxygen, it has been shown that in the CMIP5 ESMs the biogeochemical tracers are not always equilibrated with respect to the ocean circulation and a drift may be present. To account for the magnitude and sign of the model drift, in all subsequent analyses we used the preindustrial control simulations (piControl) and removed the (small) signal unrelated to externally forced centennial changes. We did so by defining, for example, $O_{2_{trend}} = O_2^{RCP8.5(B)} - O_2^{hist(A)} - \left(O_2^{piControl\ (B)} - O_2^{piControl\ (A)} \right)$, where A and B define the periods 1975–2005 and 2070–2100.

Stratification is calculated here as the potential density difference between the surface and 700 m, modifying the definition of *Capotondi et al*. [2012] relevant for tropical latitudes that considered the difference between surface and 200 m. Potential density is calculated from the modeled temperature and salinity fields using the EOS-80 polynomial. Oxygen saturation depends on temperature and salinity and is calculated based on *Garcia and Gordon* [1992]. Apparent oxygen utilization (AOU) is then determined as the difference between the O_{2sat} and O_2, which is commonly used as a measure of biological oxygen utilization. It should be noted that intense wintertime air-sea interaction often causes surface O_2 to be undersaturated leading to a nonnegligible preformed AOU [*Ito et al*., 2004], but the model outputs do not allow for a more precise estimation. The CMIP5 ESMs are compared to the climatological observations for the present climate. Annual mean climatologies from the World Ocean Atlas 2009 (WOA 2009) [*Antonov et al*., 2010; *Garcia et al*., 2010; *Locarnini et al*., 2010] are used as the observational reference of *T*, *S*, and O_2. Potential density, density stratification, oxygen saturation O_{2sat}, and AOU are calculated using the same formula. For the ocean currents, we reference to the Simple Ocean Data Assimilation (SODA) Reanalysis version 2.2.4 [*Carton et al*., 2005]. SODA 2.2.4 is based on a multivariate sequential data assimilation scheme in which *T* and *S* observations from World Ocean Database 2009 are used to update the ocean model.

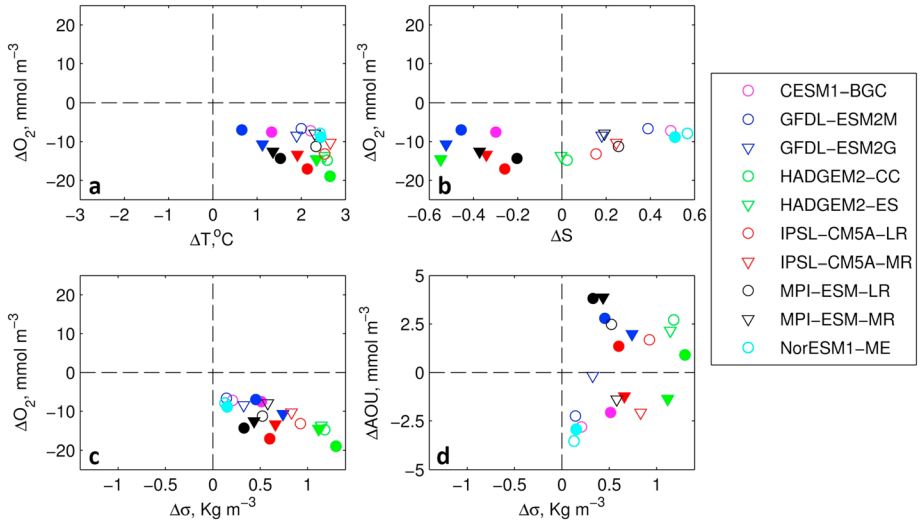

Figure 2. Spatially averaged changes of dissolved oxygen (ΔO_2) along with (a) temperature (ΔT), (b) salinity (ΔS), (c) stratification ($\Delta\sigma$), and (d) apparent oxygen utilization ΔAOU along with stratification ($\Delta\sigma$). The filled shapes represent the averaging (0–700 m) over SPNA (46°N–73°N), and the empty shapes represent the averaging over STNA (22°N–46°N).

3. Results

3.1. Model Evaluation

3.1.1. Domain-Averaged Changes

Before examining the spatial variability of the oxygen trends and their causes, we describe the time evolution of the spatially averaged (volume-weighted mean) anomalies of the quantities of interest for the entire North Atlantic (22°N–73°N; Figure 1) from 1950 to 2100. Given our focus on deep mixing and deepwater formation, we concentrate on the depth range 0–700 m. The choice of 700 m is somewhat arbitrary but represents a typical depth at which most models convect on a large enough area. The anomalies in Figure 1 are calculated on the mean state of period 1975–2005 (period A), and the climatological volume-weighted mean values from WOA are also indicated. Mean values are also shown for the projected interval 2070–2100 (period B). As expected, temperature and stratification increase and oxygen decreases in all models. The overall oxygen loss over 1950 to 2100 is in the range of 10–20 mmol m^{-3}, and is directly linked to the solubility decrease associated with the NA warming. Salinity and AOU trends, on the other hand, differ among the models and their magnitude is moderate, within (−0.35, +0.1) psu and ±5 mmol m^{-3} for the entire North Atlantic.

In Figure 2, we present the spatially averaged changes of each variable by dividing our domain in subtropical (22°N–46°N) and subpolar (46°N–73°N) regions. Both in the subpolar North Atlantic (SPNA) and subtropical North Atlantic (STNA), all of the models warm up and increase their stratification (Figures 2a and 2c). Salinity increases for all the models (Figure 2b) in the STNA region except for the HadGEM versions which freshen at the eastern subtropical gyre and show a strong zonal ΔS gradient as revealed in the following (Figure 12). In the SPNA, all the models but NorESM1-ME show negative salinity change (Figure 2b). As revealed by the spatial changes (Figure 12), NorESM1-ME significantly increases salinity in the eastern subpolar gyre counterbalancing the freshening in the rest of the subpolar region. Along with warming, stratification also increases for all of the models in the whole NA (Figure 2c). The most diverse behavior is observed in the centennial AOU changes both among the different models but also between SPNA and STNA (Figure 2d).

In this work we focus on the spatial representation of physical and biogeochemical quantities related to oxygen and we concentrate on centennial changes. Figure 1, however, shows hints of interannual variability superposed to a strong centennial trend in most variables. It remains to be determined how well CMIP5 models represent this component. Due to the limited measurements available, the temporal variability of dissolved oxygen on interannual to decadal scales cannot be easily determined over the whole North Atlantic and therefore cannot be effectively compared to that in the models. Under the assumption that the Atlantic meridional overturning circulation (AMOC) is its main driver, however, the analysis of the AMOC representation in CMIP5 has shown that most models display multidecadal variability with an approximate

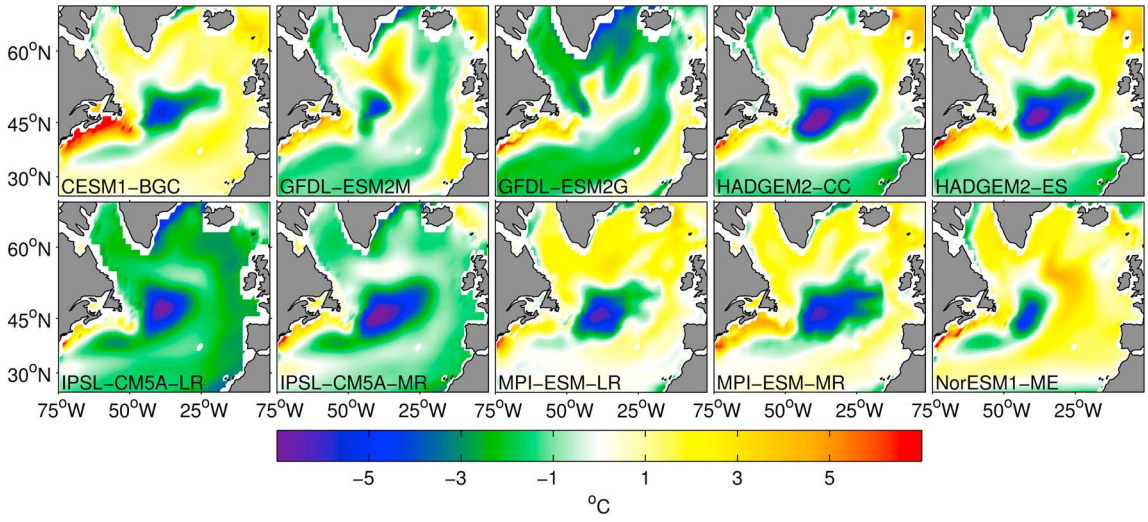

Figure 3. Mean temperature (T) bias calculated as $T^{modeled}-T^{observed}$ (from WOA09) over the period 1975–2005 depth averaged between 0 and 700 m.

60 year periodicity [*Cheng et al*., 2013] but generally underestimate the observed interannual-to-decadal changes between 1850 and 2005.

3.1.2. Biases and Climatological Spatial Fields

Next, we focus on the spatial representation of the physical and biogeochemical fields associated with oxygen variability in the North Atlantic. First, we investigate the historical period, using reanalysis products and WOA to validate the model outputs. Again, we analyze the set of variables indicated earlier and we consider their climatological means over 1975–2005 (period A) averaged over the depth range from the surface to 700 m.

Common patterns of model biases emerge in temperature (T), salinity (S), and dissolved oxygen (O_2), as shown in Figures 3–5, respectively. The most noticeable bias common to all three variables, and among all model realizations but two, is a cold, fresh, and overly oxygenated patch centered at about 48°N and 45°W. This feature is not relevant to GFDL-ESM2G and is only marginally apparent in GFDL-ESM2M. The O_2 overestimation (Figure 5) results from oxygen solubility, which reflects the cold bias in temperature. A similar pattern in the *T-S* structure was observed in the majority of the 18 global ocean-sea ice models forced by a common prescribed atmospheric state and run as part of the Coordinated Ocean-ice Reference Experiments phase II [*Danabasoglu et al*., 2014; *Griffies et al*., 2014].

The representation of the ocean circulation in the ESMs is indeed the key to explaining the model biases in T, S, and O_2 distributions. Figure 6 compares the climatological lateral circulation in the models and SODA 2.2.4 reanalysis, superimposed on the salinity distribution, both depth-averaged between the ocean surface and 700 m. The repeated solid black arrow represents the observed pathway of the North Atlantic Current (NAC) according to the SODA 2.2.4 product. The arrow follows the maxima in the depth integrated u, v fields and develops along the maximum salinity gradient. The superimposition over the individual model's circulation field (vectors) and salinity clarifies the difference between models and observation. In agreement with the analysis in *Danabasoglu et al*. [2014], the North Atlantic Current (NAC) is more zonally oriented in the ESMs relative to the observations, and the Labrador Current extends further southeast and away from the shelf, carrying cold, fresh, and highly oxygenated water into the central subpolar North Atlantic (SPNA). The zonally biased pathway of the NAC is also visible in the salinity distribution as the NAC separates the fresh subpolar waters from the salty subtropical ones. GFDL-ESM2M and GFDL-ESM2G better reproduce the NAC pathway, and as a result, the O_2 distribution in those models matches more closely the observed climatology south of Greenland.

The modeled stratification for the period of 1975–2005 is then compared with WOA in Figure 7 and used to map the areas where deep convection occurs. Locations where the vertical density gradient $\Delta\sigma$ is less than 0.5 kg m^{-3} can be used as a proxy of modeled convective areas based on a comparison with winter

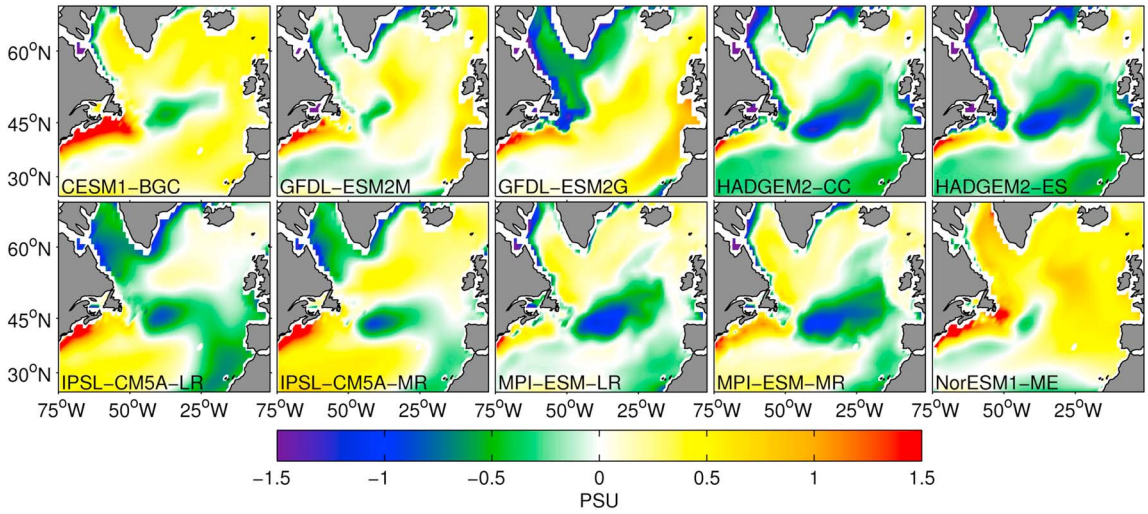

Figure 4. Mean salinity (S) bias calculated as S^{modeled}–S^{observed} (from WOA09) over the period 1975–2005 depth averaged between 0 and 700 m.

(January-February-March) mixed-layer depth performed on a subset of ESMs—six out of 10—for which monthly means of potential temperature and salinity are available over the historical period (not shown). It should be noted that when using a stratification criterion as a proxy for deep convection the convective strength cannot be quantitatively compared between two convective regions for the same model or between different models. Also, the climatological stratification of the top 700 m alone cannot inform us about the depth of convection or its seasonal cycle. No model, however, has mixed layer depth data available with monthly frequency after 2005.

With these caveats in mind, we compare the upper ocean stratification from each model to the WOA09 climatology. All CMIP5 models overestimate the stratification in the top 700 m in comparison to the WOA09 data in both the subpolar and subtropical NA. In the SPNA, where deep convection takes place, the WOA09 climatology is weakly stratified, with $\Delta\sigma < 0.5$ kg m^{-3} over a broad region extending from the Labrador and Irminger Seas to Iceland and from 70°N to 50°N. In CESM1-BGC stratification with values as low as 0.5 kg m^{-3} can be found in the eastern subpolar region extending south to 50°N and along the western and eastern coast of Greenland. Both GFDL-ESM2M and GFDL-ESM2G display a weakly stratified region

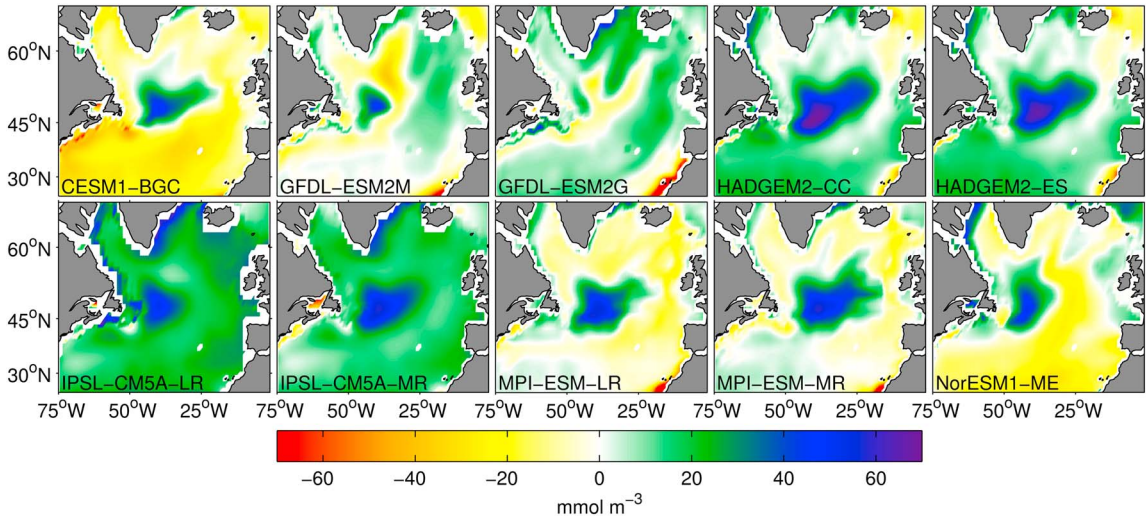

Figure 5. Mean dissolved oxygen (O_2) bias calculated as O_2^{modeled}–O_2^{observed} (from WOA09) over the period 1975–2005 depth averaged between 0 and 700 m (notice the inverted color bar).

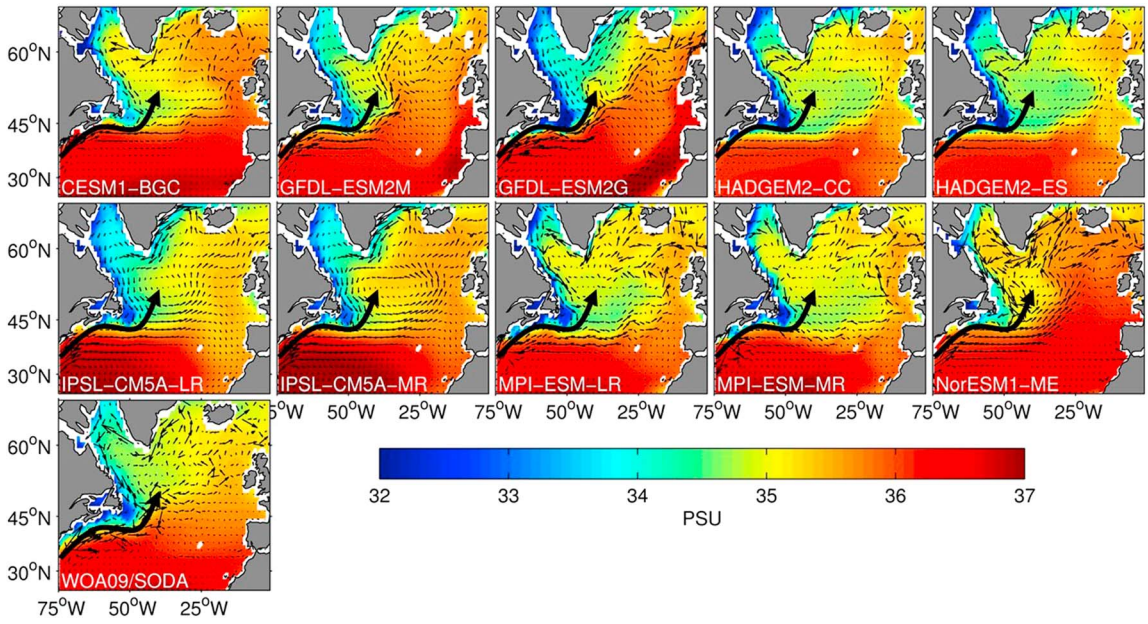

Figure 6. Time-mean salinity *S* for the period 1975–2005, averaged over 0–700 m, superposed on the depth-averaged velocity vectors for all the models and the observations (WOA09/SODA).The solid black arrow represents the observed pathway of the NAC, superimposed on the modeled circulation and salinity distribution.

over the eastern SPNA, extending to 50°N. GFDL-ESM2M is weakly stratified also in the Labrador Sea, even if less so than WOA09, while GFDL-ESM2G does not appear to convect in the LS basin. The HadGEM2-CC and HadGEM2-ES provide the most stably stratified realizations and have similar vertical structure in the upper 700 m. They both display their weakest stratification (~0.6 kg m^{-3}) in an area extending from the central LS to Iceland following the Greenland coast, and both have excess stratification biases ($\Delta\sigma > 0.9$ kgm^{-3}) in the eastern side of the subpolar gyre compared to the other models and observations. Independently of resolution IPSL-CM5A show the lowest stratification ($\Delta\sigma < 0.5$ kg m^{-3}) in the eastern SPNA. The weakly stratified

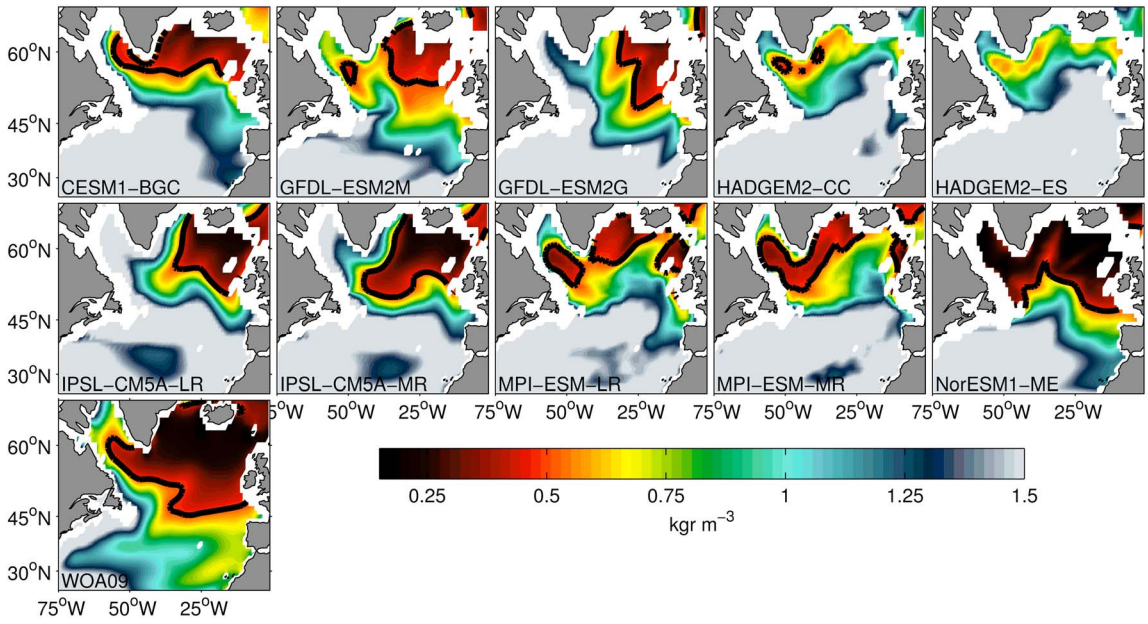

Figure 7. Time-mean stratification for the period 1975–2005, averaged over 0–700 m, defined as $\Delta\sigma = \sigma(700\text{ m}) - \sigma(10\text{ m})$. The solid black contour encloses the weakly stratified regions with $\Delta\sigma < 0.5$ kg m^{-3}, as an approximation of regions impacted by convective activity or occupied by weakly stratified waters.

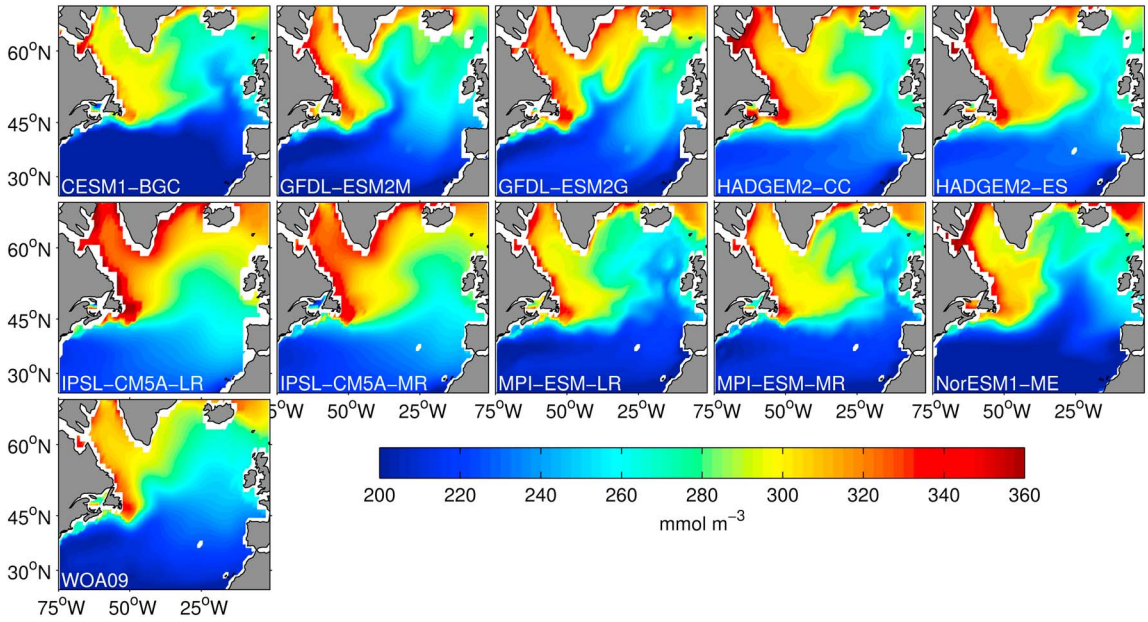

Figure 8. Time-mean 1975–2005, 0–700 m average, dissolved oxygen.

region in IPSL-CM5A-MR extends further west compared to IPSL-CM5A-LR but does not include the Labrador Sea interior. The lack of convective activity evidenced in Figure 7 in the LS in both IPSL versions, and GFDL-ESM2G is explained by the large fresh bias that characterizes these three models (Figure 4). The MPI realizations show realistic patterns, but stratification is overall too strong compared to the observations. Both MPI-ESM versions show a distinct convective region in the LS, but the eastern SPNA is too stratified south of 60°N. NorESM1-ME is weakly stratified ($\Delta\sigma < 0.5$ kg m^{-3}) over the SPNA region in a greater area than all other models.

Next, we examine the representation of dissolved O_2 concentration averaged over the top 700 m (Figure 8). There is broad agreement in the O_2 distribution despite the known biases and intermodel differences in the

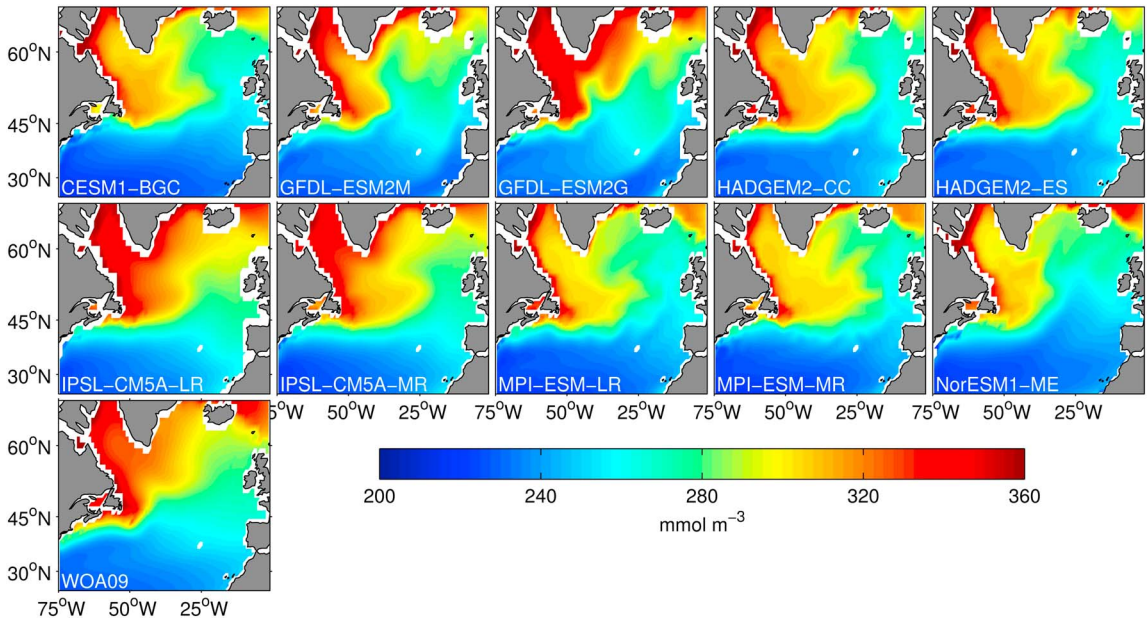

Figure 9. Time-mean 1975–2005, 0–700 m average of oxygen saturation.

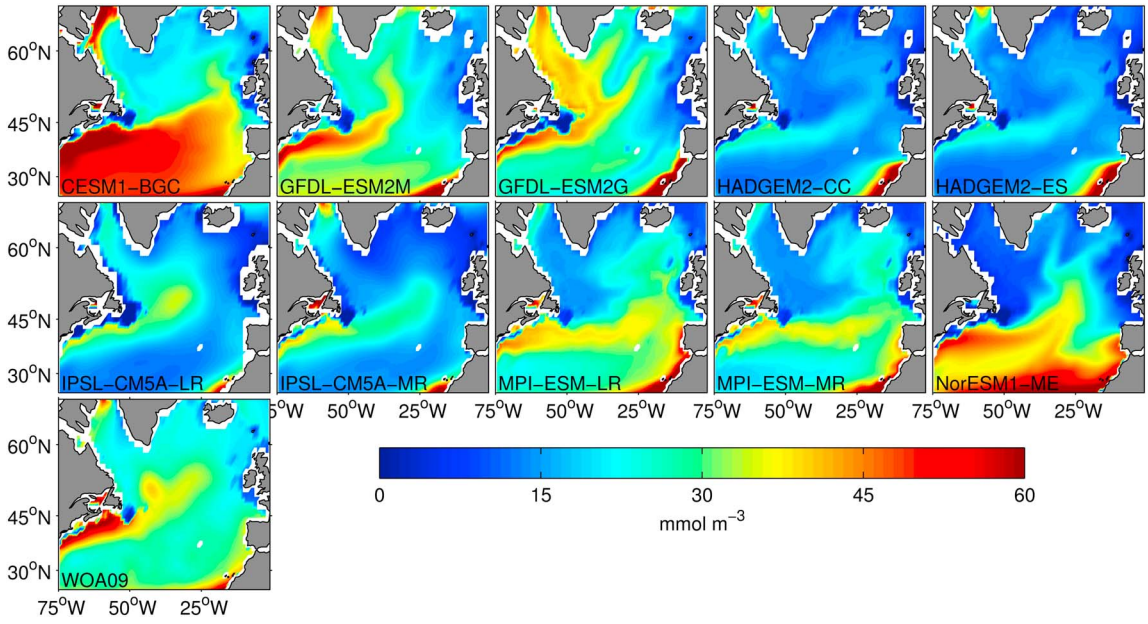

Figure 10. Time-mean 1975–2005, 0–700 m average of apparent oxygen utilization (AOU).

representation of ventilation sites and the absence of distinguishable convection in the Labrador Sea for some of the realizations. Comparing Figure 8 with Figure 9, it is evident that the relatively high O_2 in the western SPNA and the Labrador Sea primarily reflects the high solubility (O_{2sat}) associated with the cold ocean temperature in those areas.

Moving on to the AOU climatological distribution, it appears relatively homogeneous over the subtropical and subpolar region (~30 mmol m^{-3}), with maximum values found along the east coast of North America (~60 mmol m^{-3}) and off the shelf along the pathway of the NAC. Intermodel differences in AOU in the western SPNA and the Labrador Sea broadly match differences in stratification (Figure 10). In the models, convection and deepwater formation tend to decrease the regional AOU, while strongly stratified regions with a limited physical supply of O_2 are characterized by a higher AOU. The majority of the models overestimate oxygen concentration in the subtropical region south of 48°N. CESM1-BGC and NorESM1-ME are the exceptions, underestimating dissolved oxygen values by 25–45 mmol m^{-3} (Figure 8) south of 48°N. In both models the bias is due to a significant overestimation of AOU (Figure 10), and values in excess of >40 mmol m^{-3} are found in the subtropics. Both CESM1-BGC and NorESM1-ME also exhibit a strong latitudinal gradient of AOU south of 48°N. In the remaining models, patterns are in generally good agreement with the observations and present a maximum in AOU that runs from the tropics along the Gulf Stream and extends further east following the intergyre boundary and the NAC. The elevated AOU values along the Gulf Stream and the NAC are associated with the transport of high-nutrient thermocline waters, figuratively termed as the "nutrient stream" [*Letscher et al.*, 2016; *Palter et al.*, 2005; *Williams et al.*, 2011, 2006]. All models but GFDL-ESM2M and GFDL-ESM2G underestimate AOU along the northern part of the nutrient stream as a result of the O_2 overestimation, as shown in Figure 5. The near-surface portion of the nutrient stream contributes significantly to the advective nutrient supply through induction across the tilted mixed layer base. Nutrient supply across the gyre margins is dominated by lateral transport with vertical supply being secondary. As a result, the representation of the nutrient stream and associated high AOU is a crucial feature of the North Atlantic nutrient cycling.

GFDL-ESM2M and ESM2G reproduce the AOU pattern with values <40 mmol m^{-3} in the subtropical region and >50 mmol m^{-3} along the nutrient stream of the NAC. In the GFDL-ESM2G version the AOU is greater in the western subpolar region and in the LS (>45 mmol m^{-3}), compared to GFDL-ESM2M and the rest of the models. This overestimation can be attributed to its stronger stratification (Figure 7). In both versions of HadGEM the AOU values are lower than 18 mmol m^{-3} peaking along the NAC to values around

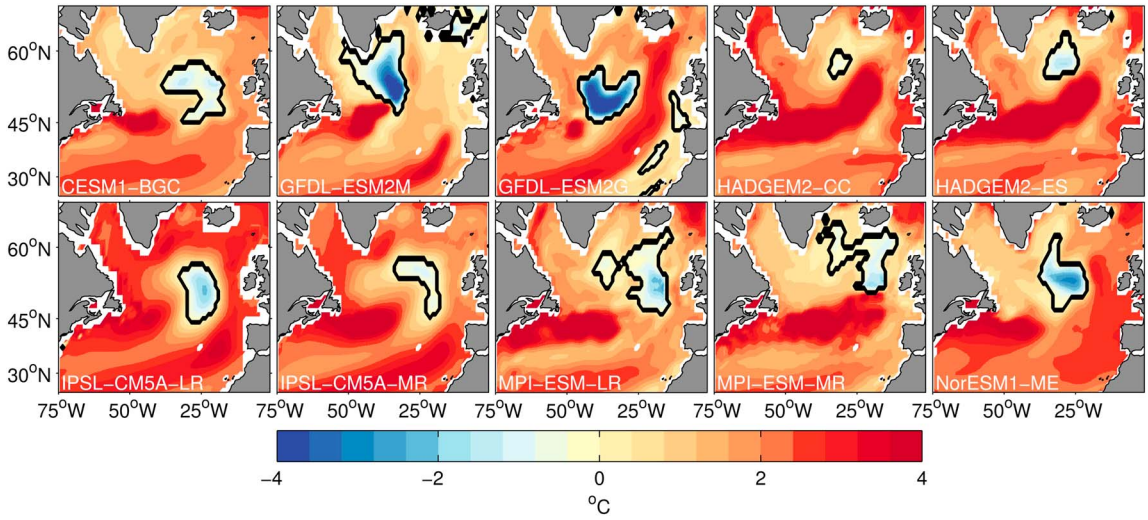

Figure 11. Centennial change of *T* calculated as the difference in 30 year averages between 2070–2100 and 1975–2005. All plotted values are 0–700 m averages. The solid black contour encloses the "warming hole."

25 mmol m^{-3}. Similarly, IPSL-CM5A shows maximum AOU of about 40 mmol m^{-3} aligned with the NAC and lower values (<20 mmol m^{-3}) north and south of it independently of resolution. In IPSL-CM5A-LR, AOU is elevated in the western SPNA and the LS compared to the MR version due to the relatively stronger stratification. Both versions of MPI-ESM-LR display AOU distributions enhanced along the NAC, with maximum values of about 40 mmol m^{-3}, in good agreement with WOA data in the subtropics, and lower than observed in the SPNA.

3.2. Spatial Patterns of the Centennial Changes

We next examine the modeled centennial changes in the North Atlantic physical and biogeochemical variables. Centennial changes are quantified considering the differences between the 2070–2100 and 1975–2005 time averages. By using 30 year averages the impact of interannual to decadal variability on the projected centennial changes is mostly averaged out. Under the Representative Concentration Pathway version 8.5 (RCP8.5) scenario, the models predict on average warmer, fresher, and more stratified waters in the SPNA. Temperature changes are shown in Figure 11 and are bounded between 1 and 4°C except for a cooling patch stretching from Greenland to the south of Iceland depending on the model.

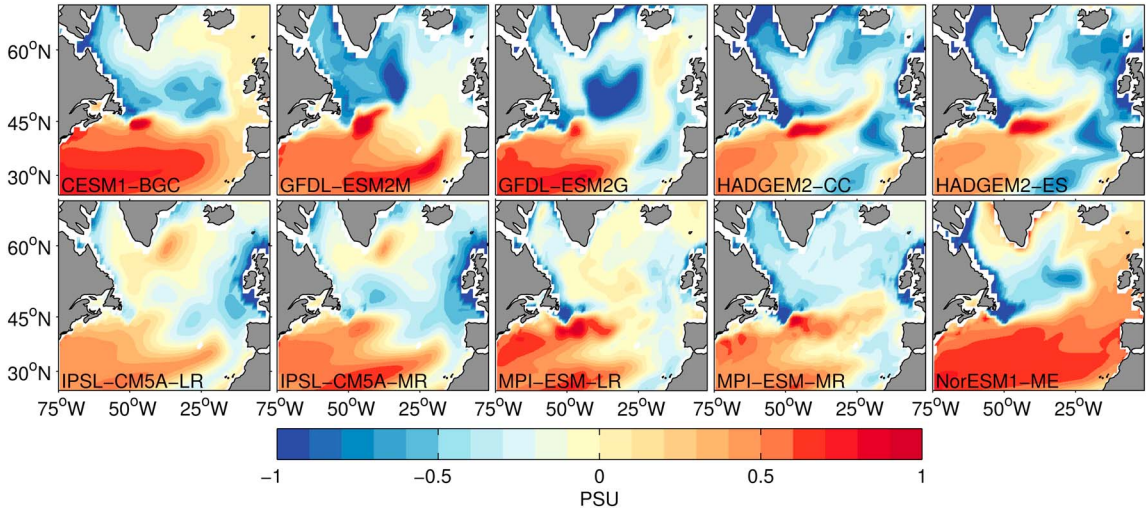

Figure 12. Centennial change of *S* calculated as the difference in 30 year averages between 2070–2100 and 1975–2005. All plotted values are 0–700 m averages.

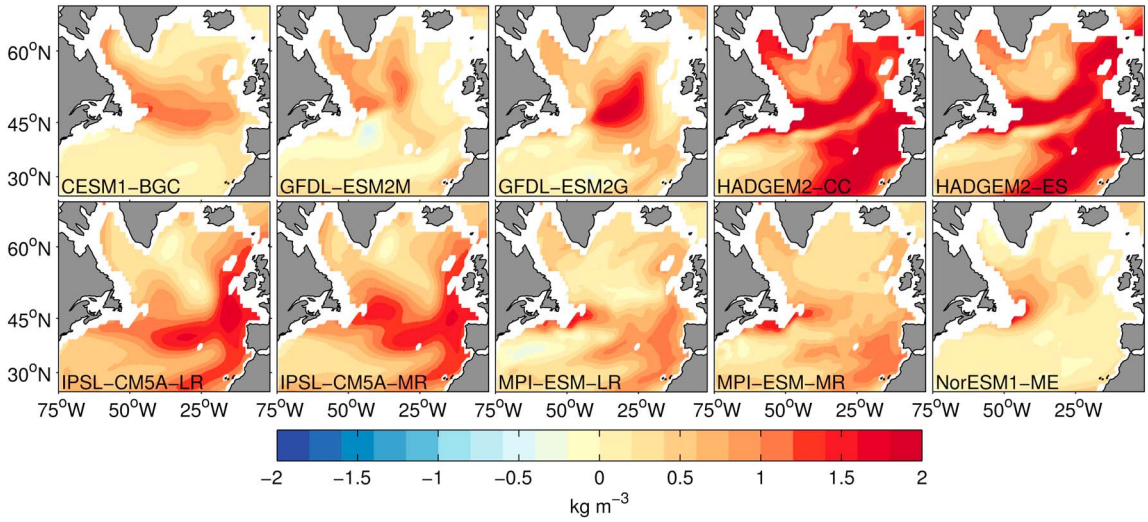

Figure 13. Centennial change of stratification calculated as the difference in 30 year averages between 2070–2100 and 1975–2005. All plotted values are 0–700 m averages.

The solid black contour in Figure 11 connects points of zero change enclosing a cooling region, a feature known in the literature as the warming hole [*Drijfhout et al*., 2012; *Rahmstorf et al*., 2015]. AMOC reduction and reduced poleward heat transport have been suggested as a possible cause for such feature, but the processes behind the warming hole are not entirely understood. This feature plays an important role in oxygen changes as we discuss later. Salinity changes are presented in Figure 12. In all models salinity increases in the subtropics, partially offsetting the warming contribution on stratification. North of 45°N the coastline surrounding the LS basin freshens in all models and freshening is also pronounced near the warming hole areas. The GFDL model shows the largest salinity decrease ($\Delta S < -1$) co-located with the warming hole, where stratification also reaches its maximum increases.

All models but NorESM1-ME predict a more stratified future state of the ocean (Figure 13) with spatially uneven changes as a result of uneven spatial warming and freshening (Figures 11 and 12). NorESM1-ME displays compensation between temperature and salinity nearly everywhere in the NA. In the SPNA, salinity

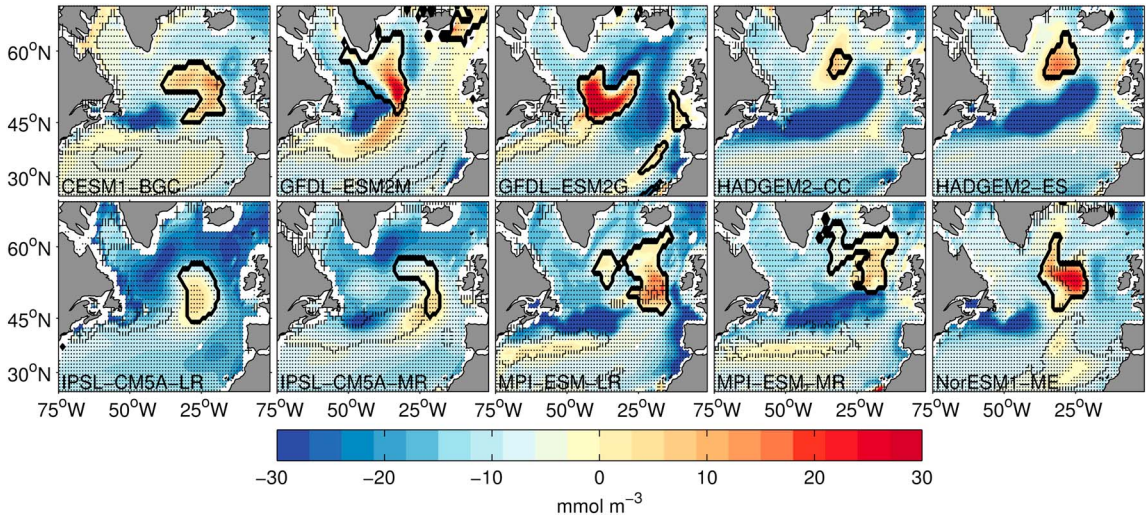

Figure 14. Centennial change of dissolved oxygen calculated as the difference in 30 year averages between 2070–2100 and 1975–2005. All plotted values are 0–700 m averages. The solid black contours enclose the "warming holes," while the dashed contours highlight the subtropical AOU decrease exceeding 1.5 times the standard deviation of negative values. The black dots indicate the areas where the results are statistically significant at the 99% confidence level according to a *t* test.

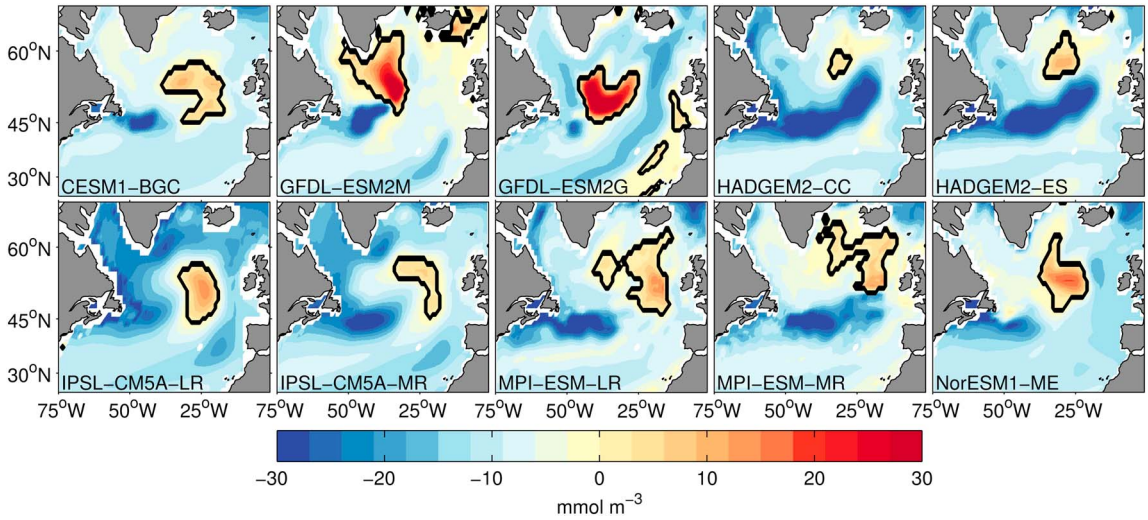

Figure 15. Centennial change of oxygen saturation calculated as the difference in 30 year averages between 2070–2100 and 1975–2005. All plotted values are 0–700 m averages.

changes contribute the most in the projected stratification state [*Fu et al*., 2015]. CESM1-BGC, GFDL-ESM2M, and both MPI versions show stratification changes within the range of 0–1 kg m^{-3}, while for the remaining the change regionally exceeds 2 kg m^{-3}. In particular, both HADGEM and IPSL versions demonstrate their maximum increase along with their biased pathway of the NAC, and at eastern subtropical gyre, with values exceeding 1.5 kg m^{-3}. These zonally oriented changes in the vertical density structure result from the northward shift of the intergyre boundary, the warm and salty Gulf Stream extension, and the NAC for those models, as revealed by the centenial changes of the kinetic energy (Figure 18). The overall positive stratification change causes a suppression of the convective regions toward the eastern subpolar NA gyre. By the end of the twenty-first century, all models are strongly stratified in the LS and lack convection in the western part of SPNA (not shown).

The increasing temperature and stratification over this century have important implications for the oxygen budget. First, the reduction of O_2 solubility can clearly be seen by comparing Figure 11 with Figure 15; the pattern of solubility change is indeed negatively correlated with that of temperature change. As expected the warming holes (marked by the solid black contours in Figure 14) are characterized by strong regional solubility increase in all models (the warming hole effect), with the GFDL ESMs leading in both temperature decrease and O_2 increase. GFDL-ESM2G exhibits a strong warming hole and oxygen increase even though it does not have a cold bias in the south of the Greenland over the historical period. While the cold bias in model climatology is still a concerning feature, the warming hole effect appears to be a robust response to greenhouse warming of all models analyzed in this study.

Second, the suppression of convective mixing at high latitudes reduces the vertical O_2 transport, leading to an increase in AOU (Figure 16) and a decrease in O_2 in the subpolar gyre (Figure 14). The quantitative relationship between AOU and stratification, however, varies among the models (Figure 15). CESM1-BGC and the two versions of the MPI models exhibit a large increase of stratification and AOU across the SPNA especially near the gyre boundary. The positions of maximum stratification (Figure 13) and AOU increase (Figure 16) are co-located in the two versions of GFDL and can be seen in the eastern part of the SPNA in the ESM2M version and in its central part in the ESM2G integration. The two versions of HADGEM2 have their maximum response in both stratification and AOU in the southeastern part of the SPNA. In contrast, in the IPSL models, the locations of maximum AOU increase are decoupled from the regions of maximum stratification change, with the first occurring in the central/eastern part of the SPNA and the second in the southeastern part of the SPNA as in the HADGEM2 runs. Many processes may be responsible for the decoupling of AOU and stratification including the responses of lateral transport, ventilation, and biological oxygen utilization to stratification changes. In the subtropics (<45°N) the AOU responses differ across models, and those differences are reflected in the O_2 changes (Figure 14). For O_2, and later for AOU, we also verified the statistical

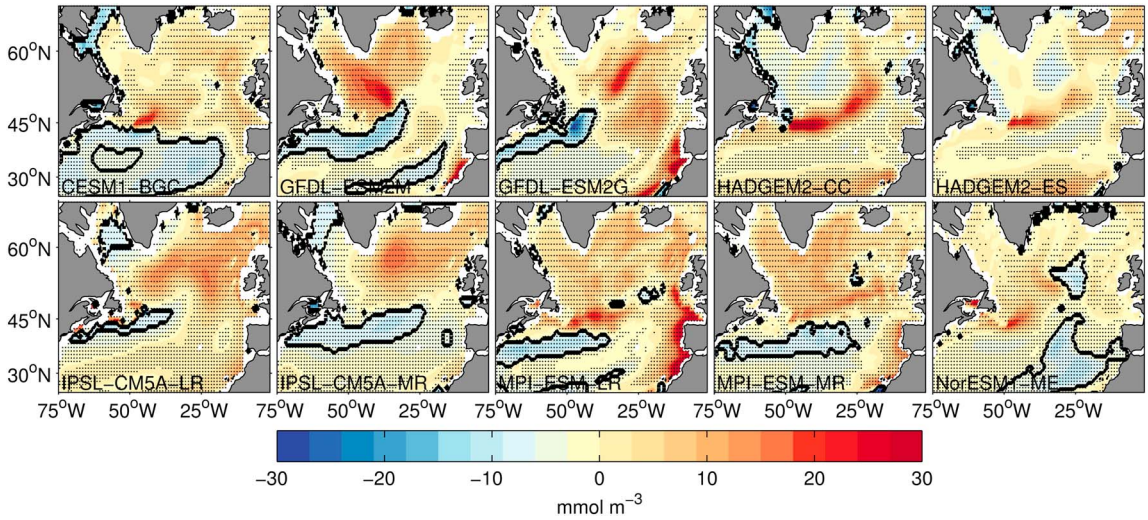

Figure 16. Centennial change of apparent oxygen utilization (AOU) calculated as the difference in 30 year averages between 2070–2100 and 1975–2005. All plotted values are 0–700 m averages. The solid black contours enclose the areas where the AOU decrease exceeds 1.5 times the standard deviation of negative values. The black dots indicate the areas where the results are statistically significant at the 99% confidence level according to a *t* test.

significance of the drift-corrected trends by testing if the average O_2 concentrations during 2070–2100 under the RCP8.5 scenario are significantly lower than those during 1975–2005 period relative to the interannual variability within each 30 year period. We used a *t* test evaluating $t = \frac{-\left\{\left(\overline{x_{\mathrm{RCP8.5}}} - \overline{x_{his}}\right) - \Delta x_{\mathrm{piControl}}\right\}}{\sigma\sqrt{\frac{1}{N_1}+\frac{1}{N_2}}}$, where σ is defined as $\sqrt{\frac{N_1 s_1^2 + N_2 s_2^2}{N_1+N_2-2}}$, and the degree of freedom is d.f. = $N_1 + N_2 - 2$ (d.f. = 58 in our case). S_1, S_2 and N_1, N_2 are the standard deviation and sample size of the periods A (1975–2005) and B (2070–2100). Preindustrial control simulations are used to correct for the model drift by subtracting their centennial changes.

In seven out of 10 models significant AOU decrease is observed along the western boundary current and in its extension along the NAC (the nutrient stream effect). The solid black contour on Figure 16 encloses the area of negative AOU change greater than the 150% of standard deviation of the negative values. The nutrient stream transports nutrient-enriched waters (high-AOU and low-oxygen) from low latitudes to subpolar

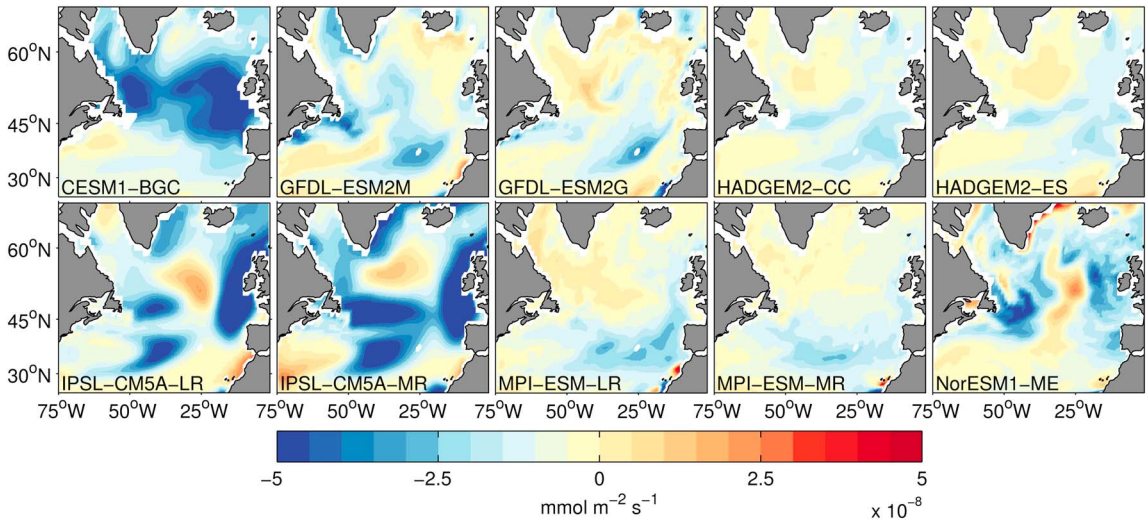

Figure 17. Centennial change of export production at 100 m depth (EP) calculated as the difference in 30 year averages between 2070–2100 and 1975–2005. The export production is expressed as the downward flux of organic carbon. All plotted values are 0–700 m averages.

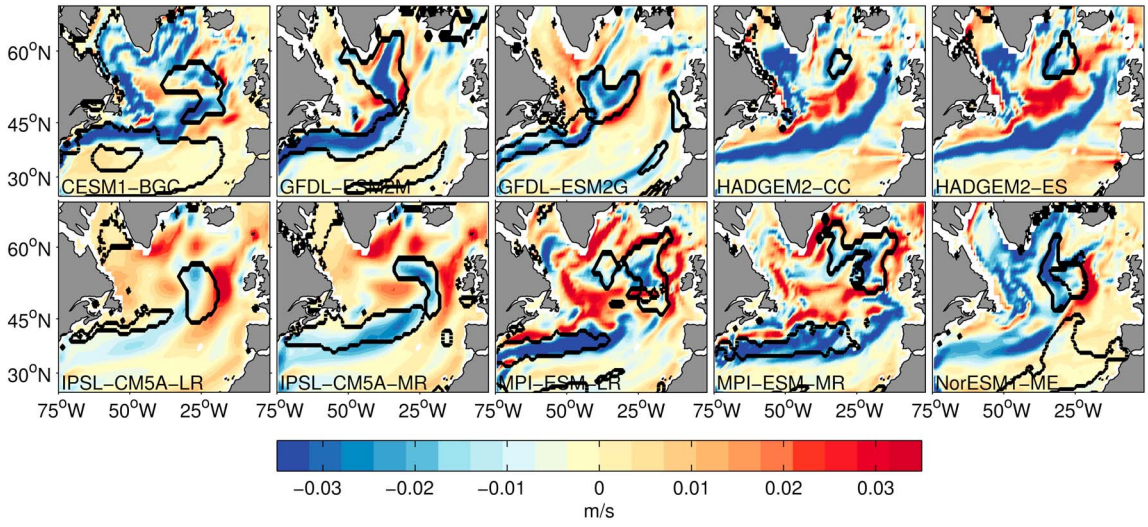

Figure 18. Centennial change of KE (cast as a speed $V_{KE} = \left(\sqrt{u^2 + v^2}\right)$) calculated as the difference in 30 year averages between 2070–2100 and 1975–2005. All plotted values are 0–700 m averages. The solid contours enclose the warming holes as defined by temperature changes, and the dashed contours enclose the areas where AOU decrease exceeds 1.5 times the standard deviation of negative ΔAOU values.

region, which weakens in the warming ocean. AOU decreases in CESM1-BGC, in the two versions of GFDL-ESMs and, even if less uniformly, in the two versions of MPI-ESMs. Consequently, in those models subtropical O_2 is resisting to deoxygenation despite the warming trend. In both versions of HADGEM2 and IPSL, on the other hand, AOU slightly increases.

Finally, biological productivity in the SPNA decreases in response to climate warming, likely due to the reduction in the vertical nutrient supply. In addition to the reduced convective mixing, a weakened AMOC may also slow down the nutrient stream of the Gulf Stream and NAC. This could potentially result in weakened export production and reduced biological consumption of subsurface O_2. The effect of biological productivity will not affect the solubility, and its impact only appears through the AOU changes. The centennial changes of AOU, therefore, reflect combined effects of convection and circulation changes, and biological oxygen consumption. A close examination of the modeled export production reveals that little agreement exists in both pattern and signs across models (Figure 17). In CESM1-BGC export production decreases over the SPNA. In the two versions of IPSL and in NorESM1-ME export production increases in the warming hole and decreases outside. The other models show a mix of moderate increase and decrease in the SPNA, and all project a decrease in export production in the eastern subtropics. Despite these intermodel differences, centennial AOU is projected to increase in the SPNA in all models, suggesting that physical processes are playing the dominant role.

The combination of the three processes outlined above explains the complex, patchy patterns of O_2 changes (Figure 14), and of the significant differences among models. Our analysis points to two major mechanisms: the thermally driven solubility trend and the change in convective activity due to the increased stratification. Some of the model-model differences can be attributed to the different representation of the warming hole and its impact on the $\Delta O_{2,\,sat}$ field. The Δ(AOU) field also display complex, variable across models, patterns. The stratification change can explain the AOU increase in the SPNA only, in particular in the southeast of Greenland and between Iceland-Scotland; however, all models but the HADGEM2 exhibit also a significant AOU decrease at the gyre boundary around 45°N, near the NAC. The AOU reduction in the vicinity of NAC occurs in all models except for the two versions of HADGEM2.

Figure 18 examines the centennial change of the mean kinetic energy (KE) in the North Atlantic and it reveals a substantial weakening of the major currents. In CESM1-BGC the NAC as well as the cyclonic circulation of the subpolar gyre weaken considerably. Both versions of GFDL show weakening of the NAC intensity without significant changes in the LS circulation. HADGEM versions show changes similar to CESM1, with weakening of the cyclonic circulation in the LS and weakening of the NAC. Increase in KE is also observed as a result of a northward shift of the NAC pathway. Such northward shift explains the zonal increase in stratification in the

HADGEM model (Figure 13) as a result of warmer and lighter waters penetrating further north in the subpolar gyre at latitudes greater than 45°N. Weakening and northward shift of the NAC is also observed in the MPI runs, but without intruding far into the subpolar gyre as in HADGEM. Both version of IPSL-CM5A project a weakening of the NAC but not as intense as in the other models.

In Figure 18 the solid contours of the "warming holes" reveal that these patchy features in the SPNA result from the slowdown of the NAC that characterizes all models and extend from the surface to 700 m and below. Around 45°N NAC changes coincide with the strongest AOU decrease, defined by the dashed contours in the subtropical region 30°N–47°N. The nutrient stream through which nutrient-enriched and oxygen-depleted waters are transported from low latitudes to the subtropical and subpolar region is therefore greatly reduced in a warming ocean.

Overall, CMIP5 ESMs display several common features in projecting the centennial-scale deoxygenation of the North Atlantic toward the end of our century. All models predict that O_2 will decrease in the subpolar region as a consequence of warming and weakened convection. Thermally driven O_{2sat} decrease and stratification-driven AOU increase will reinforce one another at subpolar latitudes. However, the projected O_2 change is not uniform in space but exhibits rather complex spatial structures. Most models exhibit strong warming near the southern boundary of the subpolar gyre (~50°N) and a strong decline of O_{2sat} there. The only patches of increasing O_2 in the subpolar regions are associated with the warming holes. At the intergyre boundary (~45°N), the magnitude of deoxygenation is reduced in all models. In about half of those we examined O_2 moderately increases along the NAC pathway. The resistance to deoxygenation is primarily due to the reduction of AOU associated with the weakened lateral transport of AOU associated with the nutrient stream. In the subtropics ($<$40°N), about half of the models predict that O_2 will regionally increase and the other half predicts that O_2 will decrease, depending on the sign of the AOU changes.

4. Conclusions

We analyzed nine ESMs from the CMIP5 catalog with various physical climate models and marine biogeochemical modules of different complexity with the goal of understanding projected dissolved oxygen changes. The ability to properly represent the North Atlantic convective regions during the historical period varies among models. For example, three of them show little to no ventilation in the Labrador Sea, and all but two models display a significant bias in the representation of the position and strength of the NAC such that the Labrador Current delivers colder, fresher, and more oxygenated waters further southeast compared to observations. Under the RCP8.5 scenario in all models the mean ocean temperature in the upper 700 m of the North Atlantic (22°N–73°N) increases by 2–4°C by the end of the twenty-first century, stratification also increases and dissolved oxygen concentrations decrease by 10–20 mmol m^{-3}. Trends in salinity and AOU, on the other hand, vary among models and between the subpolar and subtropical NA, broadly defined as north and south of 45°. These basin-scale analyses are consistent with the previous analyses of multimodel averages [*Cocco et al*., 2013; *Bopp et al*., 2013], generally following the ocean deoxygeneation hypothesis where anthropogenic warming of upper ocean leads to a decrease in the solubility of oxygen and a weakened vertical exchange due to an increased stratification.

New and unique findings of this study are the mechanisms of projected increase in the dissolved oxygen concentrations in limited areas, generally found to the south of Greenland. The existence of these patches of oxygenated waters is associated with the projected weakening of the NAC, while their locations are model-dependent due to the varied representation of the NAC pathway. This feature was not discussed in earlier studies based on multimodel averages because the patterns of oxygen change are highly model-dependent, and its signal can be obscured if averaged across many different models. However, this feature is caused by a few common mechanisms in all models. In particular, the weakening of the NAC has two distinct impacts on the projected changes in dissolved oxygen. First, reduced northward heat transport results in the models simulating a *cold temperature anomaly* in the SPNA causing a locally high oxygen concentration (the *warming hole* effect). The two versions of GFDL-ESMs are the only members in the subset considered that capture the northeastward direction of NAC in the historical runs, and project the warming hole located south of Greenland, centered at about 50°N and 45°W. The rest of the models with a strongly zonal NAC project the *hole* toward the eastern SPNA at about 50°N and between 45°W and 15°W. Those localized negative temperature changes induce a thermodynamically driven increase in dissolved

oxygen as the oxygen saturation responds to temperature. Second, reduced northward mass transport results in the AOU decrease along the pathway of the Gulf Stream extension and the NAC. The weakened advection results in the oxygen increase along its pathway because of the reduced transport of low-oxygen/high-nutrient waters from the low latitudes (the *nutrient stream* effect). Furthermore, the shift in the position of NAC causes localized, strong oxygen changes associated with the shifts in the boundaries of water masses. These localized mechanisms are operating in addition to the effects of basin-scale warming and stratification increase.

While there are differences in the detailed patterns of O_2 trend, all the ESMs agree that the basin-scale changes are primarily determined by the decline in oxygen saturation. The changes in AOU can modulate the signal but are not the determining factor for the basin-scale O_2 inventory. Despite the fact that AOU is expected to increase as a result of a more stratified ocean mean state, the changes in the circulation result in a reduction of AOU in the subtropics, leading to a relatively small change in the basin-scale AOU inventory. South of 45°N, AOU decreases for the majority of the models by 5–20 mmol m^{-3}. The weakening of the NAC causes a reduction in the lateral and vertical transport of nutrients capable of reaching the mixed layer, and this in turn results in a lower biologically driven O_2 consumption. These changes are likely explanations of the decline in the regional AOU. The western subtropical Atlantic is particularly resisting to the warming induced deoxygenation. This behavior in the subtropics is common to half of the models, suggesting a potentially important, coupled physical-biogeochemical resistance to the ocean deoxygenation in global warming scenarios. In the future research, it will also be important to determine how circulation and stratification may change whenever eddies and mesoscale variability are properly accounted for instead of simply parameterized.

In this work we pinpointed both similarities and differences across ESM model runs. The results presented here should be interpreted keeping in mind that at least three sources of uncertainties affect the projections of ecosystem stressors [*Hawkins and Sutton*, 2009]: the models' internal variability and its potential to change over long time scales (internal variability uncertainty), the different physical and biogeochemical modules and their parameterizations (model uncertainty), and the uncertainty in future emissions of greenhouse gases (scenario uncertainty). *Frölicher et al.* [2016] has shown that over centennial scales, as considered in this work, model uncertainty dominates for sea surface temperature over the subpolar North Atlantic and for O_2 over lower latitudes.

If global warming and resultant ocean heat uptake continue unabated, the O_2 saturation of the North Atlantic basin will decrease significantly in this and coming centuries. While more work is clearly needed to assess the importance of model biases in the representation of deep convection and mean currents in the future projections, our results show that the continuing warming of the SPNA will have far-reaching influence on the regional deoxygenation that will spread across other regions on the centennial time scale. Therefore, it is crucial to continue and increase data coverage of the oxygen sampling in addition to temperature and salinity so that the scientific community can better inform the public and policymakers about the progression and the potential risks of ocean deoxygenation. In this regard, further development of autonomous sensors such as Bio-Argo can provide valuable observing platform for the long-term oxygen trends.

Acknowledgments

We acknowledge the World Climate Research Programme's Working Group on Coupled Modeling, which is responsible for CMIP, and we thank the climate modeling groups (listed in Table 1 of this paper) for producing and making available their model output. For CMIP the U.S. Department of Energy's Program for Climate Model Diagnosis and Intercomparison provides coordinating support and led development of software infrastructure in partnership with the Global Organization for Earth System Science Portals. The CMIP data were obtained freely from the CMIP5 Data Access Portal (http://cmip-pcmdi.llnl.gov/cmip5/data_portal.html), and the Word Ocean Atlas Data (WOA09) were obtained from the National Center for Environmental Information (https://www.nodc.noaa.gov/OC5/SELECT/woaselect/woaselect.html). The data of the present analysis can be obtained from the authors upon request (ftagklis3@gatech.edu). We acknowledge the funding support by NSF through grant OCE-1357373 and by NOAA Climate Program Office, Climate Variability and Predictability Program, through grant NA16OAR4310173.

References

Adcroft, A., and R. Hallberg (2006), On methods for solving the oceanic equations of motion in generalized vertical coordinates, *Ocean Modell.*, *11*(1–2), 224–233, doi:10.1016/j.ocemod.2004.12.007.

Antonov, J. I., D. Seidov, T. P. Boyer, R. A. Locarnini, A. V. Mishonov, H. E. Garcia, O. K. Baranova, M. M. Zweng, and D. R. Johnson (2010), World Ocean Atlas 2009, volume 2: Salinity, in *NOAA Atlas NESDIS 69*, edited by S. Levitus, 184 pp., U.S. Gov. Print. Off., Washington, D. C.

Bentsen, M., et al. (2013), The Norwegian Earth system model, NorESM1-M—Part 1: Description and basic evaluation of the physical climate, *Geosci. Model Dev.*, *6*(3), 687–720, doi:10.5194/gmd-6-687-2013.

Boning, C. W., E. Behrens, A. Biastoch, K. Getzlaff, and J. L. Bamber (2016), Emerging impact of Greenland meltwater on deepwater formation in the North Atlantic Ocean, *Nat. Geosci.*, *9*(7), 523–527, doi:10.1038/ngeo2740.

Bopp, L., C. Le Quere, M. Heimann, A. C. Manning, and P. Monfray (2002), Climate-induced oceanic oxygen fluxes: Implications for the contemporary carbon budget, *Global Biogeochem. Cycles*, *16*(2), 1022, doi:10.1029/2001GB001445.

Bopp, L., et al. (2013), Multiple stressors of ocean ecosystems in the 21st century: Projections with CMIP5 models, *Biogeosciences*, *10*(10), 6225–6245, doi:10.5194/bg-10-6225-2013.

Bower, A. S., M. S. Lozier, S. F. Gary, and C. W. Boning (2009), Interior pathways of the North Atlantic meridional overturning circulation, *Nature*, *459*(7244), 243–247.

Canuto, V. M., A. Howard, P. Hogan, Y. Cheng, M. S. Dubovikov, and L. M. Montenegro (2004), Modeling ocean deep convection, *Ocean Modell.*, *7*(1–2), 75–95, doi:10.1016/s1463-5003(03)00038-6.

Capotondi, A., M. A. Alexander, N. A. Bond, E. N. Curchitser, and J. D. Scott (2012), Enhanced upper ocean stratification with climate change in the CMIP3 models, *J. Geophys. Res.*, *117*, C04031, doi:10.1029/2011JC007409.
Carton, J. A., B. S. Giese, and S. A. Grodsky (2005), Sea level rise and the warming of the oceans in the Simple Ocean Data Assimilation (SODA) ocean reanalysis, *J. Geophys. Res.*, *110*, C09006, doi:10.1029/2004JC002817.
Cheng, W., J. C. H. Chiang, and D. Zhang (2013), Atlantic meridional overturning circulation (AMOC) in CMIP5 models: RCP and historical simulations, *J. Clim.*, *26*(18), 7187–7197, doi:10.1175/jcli-d-12-00496.1.
Clarke, R. A., and J. C. Gascard (1983), The formation of Labrador sea-water. 1. Large-scale processes, *J. Phys. Oceanogr.*, *13*(10), 1764–1778, doi:10.1175/1520-0485(1983)013<1764:tfolsw>2.0.co;2.
Cocco, V., et al. (2013), Oxygen and indicators of stress for marine life in multi-model global warming projections, *Biogeosciences*, *10*(3), 1849–1868, doi:10.5194/bg-10-1849-2013.
Collins, W. J., et al. (2011), Development and evaluation of an Earth-system model—HadGEM2, *Geosci. Model Dev.*, *4*(4), 1051–1075, doi:10.5194/gmd-4-1051-2011.
Curry, W. B., J. C. Duplessy, L. D. Labeyrie, and N. J. Shackleton (1988), Changes in the distribution of partial derivative C-13 of deep water sigma CO_2 between the Last Glaciation and the Holocene, *Paleoceanography*, *3*, 317–341, doi:10.1029/PA003i003p00317.
Danabasoglu, G., et al. (2014), North Atlantic simulations in Coordinated Ocean-ice Reference Experiments phase II (CORE-II). Part I: Mean states, *Ocean Modell.*, *73*, 76–107, doi:10.1016/j.ocemod.2013.10.005.
Danabasoglu, G., et al. (2016), North Atlantic simulations in Coordinated Ocean-ice Reference Experiments phase II (CORE-II). Part II: Inter-annual to decadal variability, *Ocean Model.*, *97*, 65–90, doi:10.1016/j.ocemod.2015.11.007.
Dickson, R., B. Rudels, S. Dye, M. Karcher, J. Meincke, and I. Yashayaev (2007), Current estimates of freshwater flux through Arctic and subarctic seas, *Prog. Oceanogr.*, *73*(3–4), 210–230, doi:10.1016/j.pocean.2006.12.003.
Doney, S. C., et al. (2012), Climate change impacts on marine ecosystems, *Ann. Rev. Mar. Sci.*, *4*, 11–37, doi:10.1146/annurev-marine-041911-111611.
Drijfhout, S., G. J. V. Oldenborgh, and A. Cimatoribus (2012), Is a decline of AMOC causing the warming hole above the North Atlantic in observed and modeled warming patterns?, *J. Clim.*, *25*(24), 8373–8379, doi:10.1175/JCLI-D-12-00490.1.
Dufresne, J. L., et al. (2013), Climate change projections using the IPSL-CM5 Earth system model: From CMIP3 to CMIP5, *Clim. Dyn.*, *40*(9–10), 2123–2165, doi:10.1007/s00382-012-1636-1.
Dunne, J. P., et al. (2013), GFDL's ESM2 global coupled climate-carbon Earth system models. Part II: Carbon system formulation and baseline simulation characteristics, *J. Clim.*, *26*(7), 2247–2267, doi:10.1175/jcli-d-12-00150.1.
Feely, R. A., C. L. Sabine, R. Schlitzer, J. L. Bullister, S. Mecking, and D. Greeley (2004), Oxygen utilization and organic carbon remineralization in the upper water column of the Pacific Ocean, *J. Oceanogr.*, *60*(1), 45–52, doi:10.1023/B:JOCE.0000038317.01279.aa.
Frölicher, T. L., K. B. Rodgers, C. A. Stock, and W. W. L. Cheung (2016), Sources of uncertainties in 21st century projections of potential ocean ecosystem stressors, *Global Biogeochem. Cycles*, *30*, 1224–1243, doi:10.1002/2015GB005338.
Froelicher, T. L., F. Joos, G. K. Plattner, M. Steinacher, and S. C. Doney (2009), Natural variability and anthropogenic trends in oceanic oxygen in a coupled carbon cycle-climate model ensemble, *Global Biogeochem. Cycles*, *23*, GB1003, doi:10.1029/2008GB003316.
Fu, W., J. Randerson, and J. K. Moore (2015), Climate change impacts on net primary production (NPP) and export production (EP) regulated by increasing stratification and phytoplankton community structure in CMIP5 models, *Biogeosci. Discuss.*, *2015*, 12,851–12,897, doi:10.5194/bgd-12-12851-2015.
Garcia, H. E., and L. I. Gordon (1992), Oxygen solubility in seawater: Better fitting equations, *Limnol. Oceanogr.*, *37*(6), 1307–1312, doi:10.4319/lo.1992.37.6.1307.
Garcia, H. E., R. A. Locarnini, T. P. Boyer, J. I. Antonov, O. K. Baranova, M. M. Zweng, and D. R. Johnson (2010), World Ocean Atlas 2009, volume 3: Dissolved oxygen, apparent oxygen utilization, and oxygen saturation, in *NOAA Atlas NESDIS 70*, edited by S. Levitus, 344 pp., U.S. Gov. Print. Off., Washington, D. C.
Gillett, N. P., D. A. Stone, P. A. Stott, T. Nozawa, A. Y. Karpechko, G. C. Hegerl, M. F. Wehner, and P. D. Jones (2008), Attribution of polar warming to human influence, *Nat. Geosci.*, *1*(11), 750–754, doi:10.1038/ngeo338.
Giorgetta, M. A., et al. (2013), Climate and carbon cycle changes from 1850 to 2100 in MPI-ESM simulations for the Coupled Model Intercomparison Project phase 5, *J. Adv. Model. Earth Syst.*, *5*(3), 572–597, doi:10.1002/jame.20038.
Grantham, B. A., F. Chan, K. J. Nielsen, D. S. Fox, J. A. Barth, A. Huyer, J. Lubchenco, and B. A. Menge (2004), Upwelling-driven nearshore hypoxia signals ecosystem and oceanographic changes in the northeast Pacific, *Nature*, *429*(6993), 749–754, doi:10.1038/nature02605.
Gray, J. S., R. S. S. Wu, and Y. Y. Or (2002), Effects of hypoxia and organic enrichment on the coastal marine environment, *Mar. Ecol. Prog. Ser.*, *238*, 249–279, doi:10.3354/meps238249.
Griffies, S. M., et al. (2014), An assessment of global and regional sea level for years 1993–2007 in a suite of interannual CORE-II simulations, *Ocean Modell.*, *78*, 35–89, doi:10.1016/j.ocemod.2014.03.004.
Gruber, N. (2011), Warming up, turning sour, losing breath: Ocean biogeochemistry under global change, *Philos. Trans. R. Soc., A*, *369*(1943), 1980–1996, doi:10.1098/rsta.2011.0003.
Hawkins, E., and R. Sutton (2009), The potential to narrow uncertainty in regional climate predictions, *Bull. Am. Meteorol. Soc.*, *90*, 1095–1107, doi:10.1175/2009BAMS2607.1.
Ito, T., M. J. Follows, and E. A. Boyle (2004), Is AOU a good measure of respiration in the oceans?, *Geophys. Res. Lett.*, *31*, L17305, doi:10.1029/2004GL020900.
Jones, C. D., et al. (2011), The HadGEM2-ES implementation of CMIP5 centennial simulations, *Geosci. Model Dev.*, *4*(3), 543–570, doi:10.5194/gmd-4-543-2011.
Keeling, R. F., A. Koertzinger, and N. Gruber (2010), Ocean deoxygenation in a warming world, *Annu. Rev. Mar. Sci.*, *2*, 199–229, doi:10.1146/annurev.marine.010908.163855.
Kleypas, J. A., J. W. McManus, and L. A. B. Menez (1999), Environmental limits to coral reef development: Where do we draw the line?, *Am. Zool.*, *39*(1), 146–159.
Kleypas, J. A., R. A. Feely, V. J. Fabry, C. Langdon, C. L. Sabine, and L. L. Robbins (2006), Impacts of ocean acidification on coral reefs and other marine calcifiers: A guide for future research, Report of a workshop sponsored by NSF, NOAA, and the U.S. Geol. Survey. Rep., 88 pp., St. Petersburg, Fla.
Kortzinger, A., J. Schimanski, U. Send, and D. Wallace (2004), The ocean takes a deep breath, *Science*, *306*(5700), 1337–1337, doi:10.1126/science.1102557.
Lazier, J., R. Hendry, A. Clarke, I. Yashayaev, and P. Rhines (2002), Convection and restratification in the Labrador Sea, 1990–2000, *Deep Sea Res., Part I*, *49*(10), 1819–1835, doi:10.1016/s0967-0637(02)00064-x.

Lazier, J. R. N. (1980), Oceanographic conditions at Ocean Weather Ship Bravo, 1964–1974, *Atmos. Ocean*, *18*(3), 227–238, doi:10.1080/07055900.1980.9649089.

Letscher, R. T., F. Primeau, and J. K. Moore (2016), Nutrient budgets in the subtropical ocean gyres dominated by lateral transport, *Nat. Geosci.*, *9*(11), 815–819, doi:10.1038/ngeo2812.

Locarnini, R. A., A. V. Mishonov, J. I. Antonov, T. P. Boyer, H. E. Garcia, O. K. Baranova, M. M. Zweng, and D. R. Johnson (2010), World Ocean Atlas 2009, volume 1: Temperature, in *NOAA Atlas NESDIS 68*, edited by S. Levitus, 184 pp., U.S. Gov. Print. Off., Washington, D. C.

Long, M. C., K. Lindsay, S. Peacock, J. K. Moore, and S. C. Doney (2013), Twentieth-century oceanic carbon uptake and storage in CESM1(BGC), *J. Clim.*, *26*(18), 6775–6800, doi:10.1175/jcli-d-12-00184.1.

Luo, H., R. M. Castelao, A. K. Rennermalm, M. Tedesco, A. Bracco, P. L. Yager, and T. L. Mote (2016), Oceanic transport of surface meltwater from the southern Greenland ice sheet, *Nat. Geosci.*, *9*(7), 528–532, doi:10.1038/ngeo2708.

MacMartin, D. G., E. Tziperman, and L. Zanna (2013), Frequency domain multimodel analysis of the response of Atlantic meridional overturning circulation to surface forcing, *J. Clim.*, *26*(21), 8323–8340, doi:10.1175/JCLI-D-12-00717.1.

Matear, R. J., A. C. Hirst, and B. I. McNeil (2000), Changes in dissolved oxygen in the Southern Ocean with climate change, *Geochem. Geophys. Geosyst.*, *1*(11), 1050, doi:10.1029/2000GC000086.

Mernild, S. H., and G. E. Liston (2012), Greenland freshwater runoff. Part II: Distribution and trends, 1960–2010, *J. Clim.*, *25*(17), 6015–6035, doi:10.1175/jcli-d-11-00592.1.

Moore, J. K., K. Lindsay, S. C. Doney, M. C. Long, and K. Misumi (2013), Marine ecosystem dynamics and biogeochemical cycling in the community Earth system model CESM1(BGC): Comparison of the 1990s with the 2090s under the RCP4.5 and RCP8.5 scenarios, *J. Clim.*, *26*(23), 9291–9312, doi:10.1175/jcli-d-12-00566.1.

Orr, J. C., et al. (2005), Anthropogenic ocean acidification over the twenty-first century and its impact on calcifying organisms, *Nature*, *437*(7059), 681–686, doi:10.1038/nature04095.

Palter, J. B., M. S. Lozier, and R. T. Barber (2005), The effect of advection on the nutrient reservoir in the North Atlantic subtropical gyre, *Nature*, *437*(7059), 687–692, doi:10.1038/nature03969.

Plattner, G. K., F. Joos, and T. F. Stocker (2002), Revision of the global carbon budget due to changing air-sea oxygen fluxes, *Global Biogeochem. Cycles*, *16*(4), 1096, doi:10.1029/2001GB001746.

Poertner, H. O., and R. Knust (2007), Climate change affects marine fishes through the oxygen limitation of thermal tolerance, *Science*, *315*(5808), 95–97, doi:10.1126/science.1135471.

Rahmstorf, S., J. E. Box, G. Feulner, M. E. Mann, A. Robinson, S. Rutherford, and E. J. Schaffernicht (2015), Exceptional twentieth-century slowdown in Atlantic Ocean overturning circulation, *Nat. Clim. Change*, *5*(5), 475–480, doi:10.1038/nclimate2554.

Riahi, K., S. Rao, V. Krey, C. Cho, V. Chirkov, G. Fischer, G. Kindermann, N. Nakicenovic, and P. Rafaj (2011), RCP 8.5—A scenario of comparatively high greenhouse gas emissions, *Clim. Change*, *109*(1–2), 33–57, doi:10.1007/s10584-011-0149-y.

Rignot, E., J. E. Box, E. Burgess, and E. Hanna (2008), Mass balance of the Greenland ice sheet from 1958 to 2007, *Geophys. Res. Lett.*, *35*, L20502, doi:10.1029/2008GL035417.

Sarmiento, J. L., T. M. C. Hughes, R. J. Stouffer, and S. Manabe (1998), Simulated response of the ocean carbon cycle to anthropogenic climate warming, *Nature*, *393*(6682), 245–249, doi:10.1038/30455.

Stendardo, I., and N. Gruber (2012), Oxygen trends over five decades in the North Atlantic, *J. Geophys. Res.*, *117*, C11004, doi:10.1029/2012JC007909.

Stouffer, R. J., et al. (2006), Investigating the causes of the response of the thermohaline circulation to past and future climate changes, *J. Clim.*, *19*(8), 1365–1387, doi:10.1175/jcli3689.1.

Talley, L. D., and M. S. McCartney (1982), Distribution and circulation of Labrador sea-water, *J. Phys. Oceanogr.*, *12*(11), 1189–1205, doi:10.1175/1520-0485(1982)012<1189:dacols>2.0.co;2.

Taylor, K. E., R. J. Stouffer, and G. A. Meehl (2012), An overview of CMIP5 and the experiment design, *Bull. Am. Meteorol. Soc.*, *93*(4), 485–498, doi:10.1175/bams-d-11-00094.1.

van Aken, H. M., M. F. de Jong, and I. Yashayaev (2011), Decadal and multi-decadal variability of Labrador Sea water in the north-western North Atlantic Ocean derived from tracer distributions: Heat budget, ventilation, and advection, *Deep Sea Res., Part I*, *58*(5), 505–523, doi:10.1016/j.dsr.2011.02.008.

Williams, R. G., V. Roussenov, and M. J. Follows (2006), Nutrient streams and their induction into the mixed layer, *Global Biogeochem. Cycles*, *20*, GB1016, doi:10.1029/2005GB002586.

Williams, R. G., E. McDonagh, V. M. Roussenov, S. Torres-Valdes, B. King, R. Sanders, and D. A. Hansell (2011), Nutrient streams in the North Atlantic: Advective pathways of inorganic and dissolved organic nutrients, *Global Biogeochem. Cycles*, *25*, GB4008, doi:10.1029/2010GB003853.

Yashayaev, I. (2007a), Changing freshwater content: Insights from the subpolar North Atlantic and new oceanographic challenges, *Prog. Oceanogr.*, *73*(3–4), 203–209, doi:10.1016/j.pocean.2007.04.014.

Yashayaev, I. (2007b), Hydrographic changes in the Labrador Sea, 1960–2005, *Prog. Oceanogr.*, *73*(3–4), 242–276, doi:10.1016/j.pocean.2007.04.015.

Yashayaev, I., M. Bersch, and H. M. van Aken (2007), Spreading of the Labrador Sea water to the Irminger and Iceland basins, *Geophys. Res. Lett.*, *34*, L10602, doi:10.1029/2006GL028999.